PAPER • **OPEN ACCESS**

Development of bilayer tissue-engineered scaffolds: combination of 3D printing and electrospinning methodologies

To cite this article: Hilal Yilmaz *et al* 2024 *Biomed. Mater.* **19** 045029

IOP Publishing Biomed. Mater. 19 (2024) 045029 https://doi.org/10.1088/1748-605X/ad5483

Biomedical Materials

OPEN ACCESS

RECEIVED
8 January 2024

REVISED
22 May 2024

ACCEPTED FOR PUBLICATION
5 June 2024

PUBLISHED
14 June 2024

PAPER

Development of bilayer tissue-engineered scaffolds: combination of 3D printing and electrospinning methodologies

Hilal Yilmaz[1,2,3,*], **Tuba Bedir**[1,4], **Sevda Gursoy**[1,2,3], **Elif Kaya**[5], **Ilkay Senel**[3], **Gulgun Bosgelmez Tinaz**[2,5], **Oguzhan Gunduz**[1,2,4] and **Cem Bulent Ustundag**[2,3]

[1] Center for Nanotechnology & Biomaterials Application and Research (NBUAM), Marmara University, Istanbul, Turkey
[2] Health Biotechnology Center for Excellence Joint Practice and Research (SABIOTEK), Yildiz Technical University, Istanbul, Turkey
[3] Department of Bioengineering, Faculty of Chemical and Metallurgical Engineering, Yildiz Technical University, Istanbul, Turkey
[4] Department of Metallurgical and Materials Engineering, Faculty of Technology, Marmara University, Istanbul, Turkey
[5] Department of Basic Pharmaceutical Sciences, Faculty of Pharmacy, Marmara University, Istanbul, Turkey
[*] Author to whom any correspondence should be addressed.

E-mail: hilaltoptas44@gmail.com

Keywords: bilayer scaffold, gelatin methacryloyl, ciprofloxacin, polycaprolactone, collagen, tissue engineering

Abstract

Although different fabrication methods and biomaterials are used in scaffold development, hydrogels and electrospun materials that provide the closest environment to the extracellular matrix have recently attracted considerable interest in tissue engineering applications. However, some of the limitations encountered in the application of these methods alone in scaffold fabrication have increased the tendency to use these methods together. In this study, a bilayer scaffold was developed using 3D-printed gelatin methacryloyl (GelMA) hydrogel containing ciprofloxacin (CIP) and electrospun polycaprolactone (PCL)-collagen (COL) patches. The bilayer scaffolds were characterized in terms of chemical, morphological, mechanical, swelling, and degradation properties; drug release, antibacterial properties, and cytocompatibility of the scaffolds were also studied. In conclusion, bilayer GelMA-CIP/PCL-COL scaffolds, which exhibit sufficient porosity, mechanical strength, and antibacterial properties and also support cell growth, are promising potential substitutes in tissue engineering applications.

1. Introduction

Cells within tissues are surrounded by three-dimensional structures with a wide range of properties and sizes ranging from a few nanometers to hundreds of micrometers. Highly complex hierarchical structures are common in most biological tissues. Although the fabrication of such hierarchical structures in natural tissues remains complex and highly challenging for tissue engineering [1], numerous publications demonstrate a high degree of biomimicry in terms of microstructures. In order to reconstruct biological systems, different natural hierarchical levels need to be artificially mimicked. For this reason, the development of composite structures to synthetically shape biomimetic scaffolds produced in a controlled and reproducible manner while mimicking the hierarchical structure of tissues has become a recent trend [2]. Researchers have suggested that the combination of materials and production methods can be an effective way to improve the performance of biomaterials [3]. The most prominent approach is hydrogel/nanofiber composites, which have made significant progress in biomedical fields such as tissue engineering, regenerative medicine, and drug delivery [4]. In this context, many studies have focused on the preparation of hydrogel electrospun composite structures to simulate native extracellular matrix (ECM) [3]. This approach, which allows for biomimetic design, targets the cell-material interaction and determines the most appropriate biomaterials to fabricate specialized scaffolds. Recently, there has been an increasing number of studies on the fabrication of hydrogel/nanofiber composites by combining 3D printing and electrospinning techniques [4]. There are many different design and fabrication methods for hydrogel/nanofiber composites, such as 'simultaneous electrospinning/electrospraying technique, electrospinning technology combined with 3D printing, hydrogel components electrospun coaxially with

other components, hydrogel precursor used as electrospinning solution, and laminated hydrogel with electrospun nanofibers' [4]. The aim of this combination of methods is to produce multilayer nanofibers by electrospinning on hydrogel structures produced by 3D printing technology. Thus, the hydrogel in this composite structure is 3D printed to a specific hardness and geometry and retains its strong water absorption and expansion properties. In addition, the nanofibers have a high surface-to-volume ratio and can support cell penetration and nutrient exchange and improve mechanical properties [5, 6].

The aim of this study was to develop an alternative approach to the fabrication of biomimetic scaffolds by fabricating 3D printed GelMA using the DLP method and PCL-COL nanofibers using electrospinning to develop hydrogel/nanofiber composites. The goal is to fabricate structures of macroscopic complexity using these two methods. The continued development of new interactive chemistries, materials, and manufacturing processes will help advance the field by integrating and applying them to functional tissue engineering materials.

According to the American Society for Testing and Materials standard classification, there are seven basic 3D printing techniques. These are: material jetting, material extrusion, binder jetting, vat photopolymerization, powder bed fusion, sheet lamination, and directed energy deposition techniques. Each type of 3D printing technique has its own advantages and limitations, and the selection of an appropriate 3D printing technique depends largely on the intended application. Vat photopolymerization is the third most commonly used 3D printing technique with a rate of 16.52%. This technique can be used to fabricate various tissues such as bone, cartilage, nerve, liver, and skin, as well as various medical devices. Natural and synthetic polymers, ceramics, and metals can be used as resins. In this printing method, the photocurable resin is selectively cross-linked when a light source is projected onto the surface to initiate the free-radical photopolymerization process to obtain 3D parts of the desired product [7]. Vat photopolymerization process; It can be categorized as top-down or bottom-up depending on the location of the light source, and can be divided into two main groups: stereolithography (SLA) and digital light processing (DLP). DLP is therefore an advanced version of SLA. It is based on the principle of layer-by-layer curing of photopolymer resins [8]. Significantly faster production is achieved with DLP. This ensures adequate macromer conversion with an optimal exposure time, while minimizing overexposure to prevent unwanted partial polymerization of the surrounding resin [9]. This method reduces process time, allows high-resolution fabrication, and produces structures with perfect geometries that mimic natural tissues [7, 10, 11]. Currently, while many photoreactive biomaterials are used in light-based 3D bioprinting, gelatin methacryloyl (GelMA) is the most preferred biomaterial due to its properties such as printability, biocompatibility, and biodegradability [12]. GelMA's excellent biocompatibility, tunable physical and chemical properties, or ease of biological modification have made it an attractive choice for the biofabrication of various tissues or organs [13]. GelMA is formed by the modification of gelatin with photocrosslinkable methacrylamide groups. However, its poor mechanical properties alone limit its application. Various methods of hydrogel preparation have been proposed to increase mechanical strength [9, 14]. Song *et al* GelMA/HAp porous composite scaffolds developed by DLP method have developed a product with good mechanical properties, printability and potential for osteogenic activity to be used in bone repair [15]. Gao *et al* They reported that they improved chondrogenic differentiation and facilitated vascularization and bone remodeling by fabricating GelMA-PMAA scaffolds developed by the DLP method for bone regeneration by endochondral ossification [16]. Qian *et al* As a result of their in vivo studies with hDPSC-loaded GelMA microspheres developed by the DLP method for dental pulp regeneration, they reported the development of odontoblast-like cells in the highly vascularized dental pulp and root canals of incisors [17]. Shen *et al* They reported the GelMA/SG scaffold developed using the DLP method, which has mechanical and biological properties suitable for cartilage repair [18]. Joshi *et al* They reported successful wound treatment using the modified GelMA micropyramidal dressing developed using the DLP method [19].

On the other hand, electrospinning is one of the most successful techniques for the fabrication of three-dimensional, porous, and nano/micron-scale fiber-based matrices with tunable morphology [20, 21]. Electrospun membranes contain nanofibers with high surface area-to-volume ratios, providing abundant protein adsorption sites and numerous cell attachment sites [20]. In this study, polycaprolactone (PCL) was chosen for its mechanical strength and hardness to produce membranes by using electrospinning method. PCL is hydrophobic, making this biomaterial alone unsuitable for cell affinity and artificial tissue formation [22, 23]. Electrospun fibers can combine the biocompatibility of natural polymers with the superior mechanical strength of synthetic polymers [20]. Collagen (COL), the major component of the ECM, is highly hydrophilic and has good biodegradability and biocompatibility. It supports proliferation and differentiation by promoting cell attachment [24]. The disadvantages of PCL can be overcome by creating a PCL-COL composite [25]. Thus, it can further affect the mechanical properties, plasticity, biocompatibility, and degradability of the nanofiber, and thus the repair efficiency of the tissue

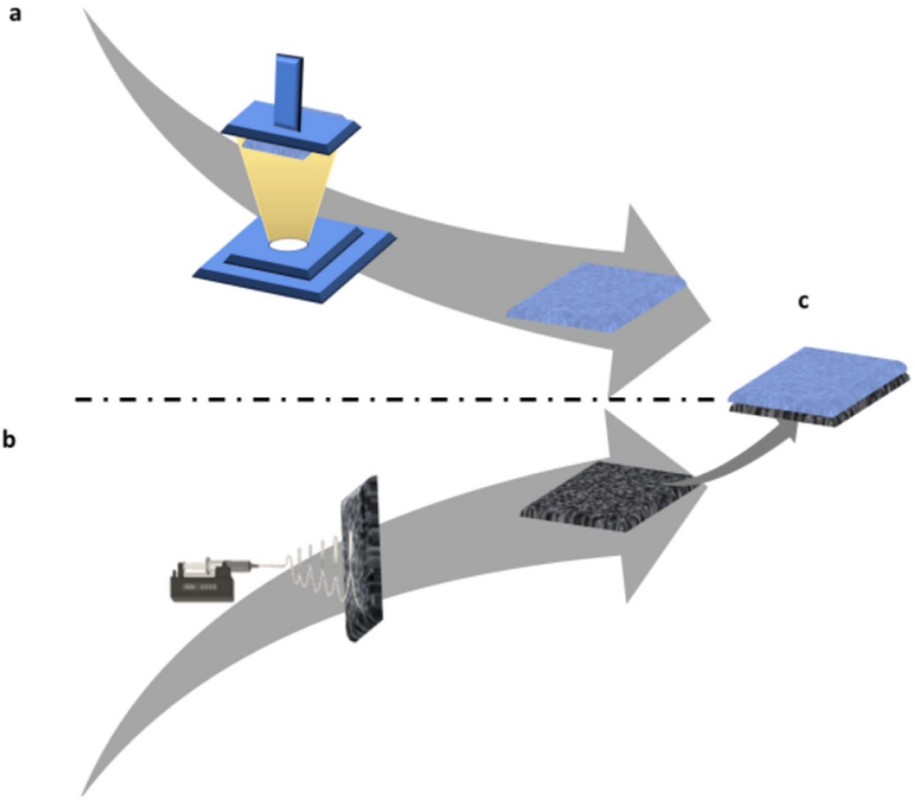

Figure 1. Schematic illustration of the development process of bilayer GelMA-CIP/PCL-COL scaffolds: (a) DLP printing of GelMA-CIP hydrogel, (b) Preparation of PCL-COL nanofiber, (c) Bilayer scaffold.

[26]. PCL-COL nanofibers are also used in many areas of tissue engineering, such as wound dressing [27], vascular graft [28], bone and cartilage [26], and drug delivery system [29] are also used.

This study presents a bilayer scaffold design consisting of 3D-printed hydrogel/electrospun nanofiber that can mimic natural tissue for use in tissue engineering. First, GelMA hydrogels containing ciprofloxacin (CIP) were developed using the DLP 3D printing method. CIP, an FDA-approved broad-spectrum antibiotic known to be effective against gram-negative and some gram-positive bacteria, was incorporated into the GelMA hydrogel to provide antibacterial properties [30, 31]. Thus, within the scope of this study, the product produced by the 3D printing and electrospinning approach can be used for interface tissue engineering (ITE). The ligament-cartilage region can also be included in the most studied ligament-bone, tendon-bone, and cartilage-bone interface tissues [32], which are found in the living body and can be used in the production of biological artificial tissue alternatives to renew or completely repair the functions of damaged or diseased areas at the interface in these areas.

To the best of our knowledge, a bilayer scaffold consisting of 3D-printed GelMA-CIP hydrogel and electrospun PCL-COL nanofibers has been developed for the first time in the literature for tissue engineering applications. The chemical, morphological, and mechanical properties of the developed bilayer GelMA-CIP/PCL-COL scaffolds were studied, and their drug release behavior, antimicrobial properties, and cytocompatibility were investigated *in vitro*. This innovative bilayer scaffold can present a promising and effective treatment approach for addressing tissue engineering (figure 1).

2. Materials and Methods

2.1. Materials

Gelatin type B from bovine skin and COL was bought from Halavet (Turkey). Ciprofloxcacin was purchased from Cayman Chemical (USA). PCL (M_w = 80.000 g mol^{-1}), methacrylic anhydride (MAA), lithium phenyl-2,4,6-trimethyl-benzoyl phosphinate (LAP), and dialysis membrane (cut-off value 14 kDa and average flat width 43 mm) were obtained from Sigma–Aldrich (Darmstadt, Germany). Sodium carbonate, sodium hydroxide, hydrochloric acid fuming 37%, and Parafilm® M were purchased from Merck (Darmstadt, Germany). Phosphate-buffered saline (PBS, pH 7.4) was bought from ChemBio (Turkey). Sodium hydrogen carbonate (>99.7%) was purchased from ISOLAB (Eschau, Germany).

2.2. GelMA synthesis

GelMA was synthesized following a previously established protocol [33]. Briefly, a 10% (w/v) gelatin solution was allowed to dissolve in 0.1 M bicarbonate buffer (pH 9) at 60 °C. Subsequently, 0.2 ml of MAA per gram of gelatin was added to the gelatin solution and reacted for 3 h at 50 °C with constant stirring. Next, the pH was adjusted to 7.4 to terminate the reaction. The resulting solution was dialyzed in distilled water at 40 °C for 5 d to remove unreacted MAA and methacrylic acid by-products. It was then lyophilized for 3 d and stored at −20 °C until use.

2.3. Preparation of GelMA-CIP solution

0.4 g of GelMA was dissolved in PBS (pH 7.4) at 50 °C to obtain a 20% (w/v) GelMA solution. Next, an antibiotic stock was prepared by adding 0.5 mg of CIP in 10 ml of 1 N HCl. Then, different concentrations of antibiotic solution (30, 100, 250, 500 μl) were prepared to be added to the GelMA solution. As a result of the optimization studies, 500 µl of CIP was added to the GelMA solution. Subsequently, 0.25% (w/v) of the photoinitiator (LAP) was incorporated into the obtained solution. Following this, the mixture was poured into the tank of the 3D printer.

2.4. Design and DLP printing of GelMA-CIP hydrogel

For the 3D printing process, a model with a thickness of 3 mm and a base of 10 × 10 mm was designed using the computer-aided design software SolidWorks 2020 (Dassault Systèmes SE, Vélizy-Villacoublay, France). The design was converted to *.stl* file format and sliced using the 3D printer software Chitubox (Shenzhen Chuangbide Technology Co., Ltd, Shenzhen City, China). A 3D printer (Phrozen Shuffle 4 K, Phrozen Tech Co. Ltd, Hsinchu, Taiwan) with a 60 s exposure time, 12 mW cm^{-2} light intensity, and 405 nm light wavelength was used. The produced 3D-printed hydrogel was kept at −20 °C for 1 d, then dried in a lyophilizer for 1 d, and stored in a container at room temperature until characterization.

2.5. Preparation of PCL-COL solutions and electrospinning process

To prepare electrospinning solutions, 15% (w/v) PCL and 15/5% (w/v) PCL/COL solutions were dissolved in a 90% acetic acid solution at 450 rpm for 24 h. Next, the solutions were fed into 10 ml plastic syringes connected to the 21-gauge metal needle. A laboratory-scale device (NS24, Inovenso Co., Turkey) was used to produce PCL and PCL/COL nanofibers. Experimental parameters for the electrospinning process were optimized to be 18 kV voltage, 1 ml h^{-1} flow rate, and 12.5 cm distance between the needle tip and collector. All electrospinning processes were performed under ambient conditions.

To obtain a bilayer scaffold, nanofibers were cut in 10 × 10 dimensions after the electrospinning process. Then, when the hydrogels produced by 3D printing were wet, the hydrogel layers were adhered to each other with the nanofibers prepared.

2.6. Scanning electron microscopy

The surface morphology of the GelMA, GelMA-CIP hydrogels, PCL, PCL-COL nanofibers, GelMA/PCL and GelMA-CIP/PCL-COL scaffolds was examined using a scanning electron microscope (EVA MA 10, Zeiss, Jena, Germany). The specimens were coated with gold for 120 s using a spray coating machine (SC7620, Quorum, Laughton, East Sussex, UK). Histogram graphs from scanning electron microscopy (SEM) results of hydrogels and nanofiber were drawn using imaging software (Olympus Analysıs, USA).

2.7. Fourier transform infrared spectroscopy

Fourier transform infrared spectroscopy (FTIR, FT/IR-ATR 4700, Jasco, Easton, MD, USA) was used to determine the chemical structure of CIP, gelatin, GelMA, GelMA-CIP hydrogels, PCL, COL, and PCL-COL nanofibers. Measurements were performed at room temperature with a resolution of 4 cm^{-1} in the wavelength range 450–4000 cm^{-1}.

2.8. Mechanical characterization of scaffolds

The mechanical properties of GelMA, GelMA-CIP hydrogels, PCL, PCL-COL nanofibers, GelMA/PCL and GelMA-CIP/PCL-COL bilayer scaffolds were studied using a mechanical testing machine (EZ-LX, Shimadzu, Kyoto, Japan). The compression test was applied to hydrogel samples; cylindrical hydrogels 6 mm in height and 8 mm in diameter were printed for the test. The compression tests were carried out at a rate of 1 mm per minute up to a maximum of 50% strain. The tensile test was conducted on the nanofiber and bilayer scaffold samples. Before tensile tests, the thickness of 10 × 50 mm nanofiber samples was measured using a digital micrometre (Mitutoyo MTI Corp., USA). The tensile tests were carried out with a load cell of 5 kN ± 0.5% at a speed of 5 mm min^{-1} and with a displacement resolution of 1 µm at room temperature (23 °C).

2.9. Swelling and degradation behaviour of scaffolds

Swelling measurements were performed to determine the water uptake capacity of the hydrogels, nanofibers and bilayer scaffolds in PBS at pH 7.4. During the test, the initial weights (W_0) of the hydrogels and nanofibers were recorded. The samples were then transferred to Eppendorf tubes containing 2 ml of PBS and kept at 37 °C in a thermal shaker (Microtest). After a certain time (5, 15, 30, 45, 60, and 90 min for hydrogels; 1, 3, 5, 12, 24, 48, and 96 h for nanofibers; 5, 15,

30, 45, 60, 90 and 180 min for bilayer scaffolds), the samples were removed from the excess water, and the wet weight (W_w) of the samples was measured. The swelling ratio was calculated using equation (1):

$$\text{Swelling ratio } (\%) = \frac{Ww - W_0}{W_0} \times 100\%. \quad (1)$$

Hydrogels and nanofibers were weighed for degradation tests and placed in 2 ml of PBS at 37 °C. After a certain time (1, 3, 7, 14, and 21 d for hydrogels; 1, 7, 14, and 21 d for nanofibers), the samples were separated from PBS and dried for 24 h. The dried weight (W_t) of the samples was measured and the degradation rate was calculated according to equation (2):

$$\text{Degradation rate } (\%) = \frac{W_0 - W_t}{W_0} \times 100\%. \quad (2)$$

2.10. *In vitro* drug release study

By measuring the UV–vis absorption of the drug in PBS (pH 7.4) at predetermined time intervals, the release profile of CIP from the GelMA-CIP hydrogels was investigated. First, the CIP linear calibration curve was analyzed using a UV-vis spectrophotometer (Jenway 7315, Bibby Scientific, Staffordshire, UK) at 278 nm. Next, the samples were kept at 37 °C in 2 ml of PBS. At predetermined time points (0.25, 0.5, 1, 2, 3, 4, 6, 8, 12, 24 and 48 h), samples were removed from the PBS, transferred to a UV–vis spectrophotometer, and the amount of drug release was measured. Then, the samples were replaced with a fresh buffer solution for the continuation of the release studies.

2.11. *In vitro* antibacterial activity

The Clinical Laboratory Standards Institute disc diffusion method was used to evaluate the antibacterial activity of GelMA-CIP hydrogels against *Staphylococcus aureus ATCC 25 923, Escherichia coli ATCC 25 922*, and *Pseudomonas aeruginosa ATCC 27 853*. Overnight cultures of *S. aureus ATCC 25 923, E. coli ATCC 25 922*, and *P. aeruginosa ATCC 27 853* were spread on Mueller–Hinton agar plates. GelMA-CIP hydrogels cut into 6-mm slices were then placed on the agar plates and incubated at 37 °C for 24 h. By measuring the zone diameters, the inhibition zones around the disks were determined. Drug release studies were carried out according to the most effective drug concentration determined as a result of antimicrobial analysis.

2.12. *In vitro* cell viability

Mouse fibroblast L929 cells (NCTC clone 929; American Type Culture Collection (ATCC, VA, USA; ECACC No. 2869501)) were used to determine *in vitro* cell viability. Cells were cultured in DMEM containing 10% FBS and 1% penicillin-streptomycin in a 5% CO_2, 37 °C incubator. The cells were observed under an inverted microscope, and the medium was changed approximately every 3 d. When the cell layer was close to 80%, cells were detached from the medium with a trypsin solution and incubated in a 96-well plate. The cells were observed under an inverted microscope (Zeiss Axio Observer Z1) GelMA, GelMA-CIP hydrogels, PCL, PCL-COL nanofibers, and GelMA/PCL, bilayer GelMA-CIP/PCL-COL scaffolds were investigated for cell viability and UV sterilized for 1 h before the MTT assay. After sterilization, all were placed in a 96-well plate and incubated with 2×10^4 cells per well. Cells were incubated on the biomaterials for 7 d. To determine cell viability, MTT analysis, a colorimetric method, was performed on days 1, 3, and 7. Briefly, 10 µl of MTT solution (5 mg MTT ml^{-1} in PBS) was added to the wells to be assayed and allowed to form formazan crystals for 3 h at 37 °C. Then 100 µl of DMSO was added to each well to solubilize the formazan crystals. The optical density (OD) at 570 nm was measured using an Elisa reader (Thermoscientific Multiskan GO). Only DMSO-treated cells were used as the positive control, while only monolayer cells not seeded on the biomaterial were used as the negative control. The percentage of cell viability was calculated for all cell culture methods. Cell viability (100%) was measured using equation (3):

$$\text{Cell viability } (\%) = \frac{\text{OD treatment}}{\text{OD control}} \times 100\%. \quad (3)$$

3. Results and Discussion

3.1. Scanning electron microscopy

The morphology of the hydrogels and nanofibers was examined by Scanning electron microscopy (SEM) analysis, and the micrographs are shown in figure 2. In addition, the general view of the bilayer scaffold consisting of hydrogel and nanofiber layers is shown in figure 2(a). The pore size in hydrogels is an important parameter that affects the degradation profile, drug transport, and high cellular activities including cell penetration and differentiation [34]. The average pore diameters of GelMA and GelMA-CIP hydrogels were measured to be 10.42 ± 6.519 µm and 4.26 ± 2.331 µm, respectively (figures 2(b) and (c)). The addition of CIP reduced the matrix density of GelMA hydrogel, making it more porous. According to these results, it can be said that GelMA-CIP hydrogel has a more porous structure than GelMA, but its pore diameters are smaller. This can be attributed to the fact that it changes the mechanics of GelMA-CIP hydrogel by causing a decrease in the polymer chain. Moreover, this may be because HCl in the CIP solution can lower the acidity of the medium and protonate the amine groups ($–NH_2$) in the backbone of the gelatin hydrogel [35]. Based on these findings, the pore sizes of the produced hydrogels are suitable for

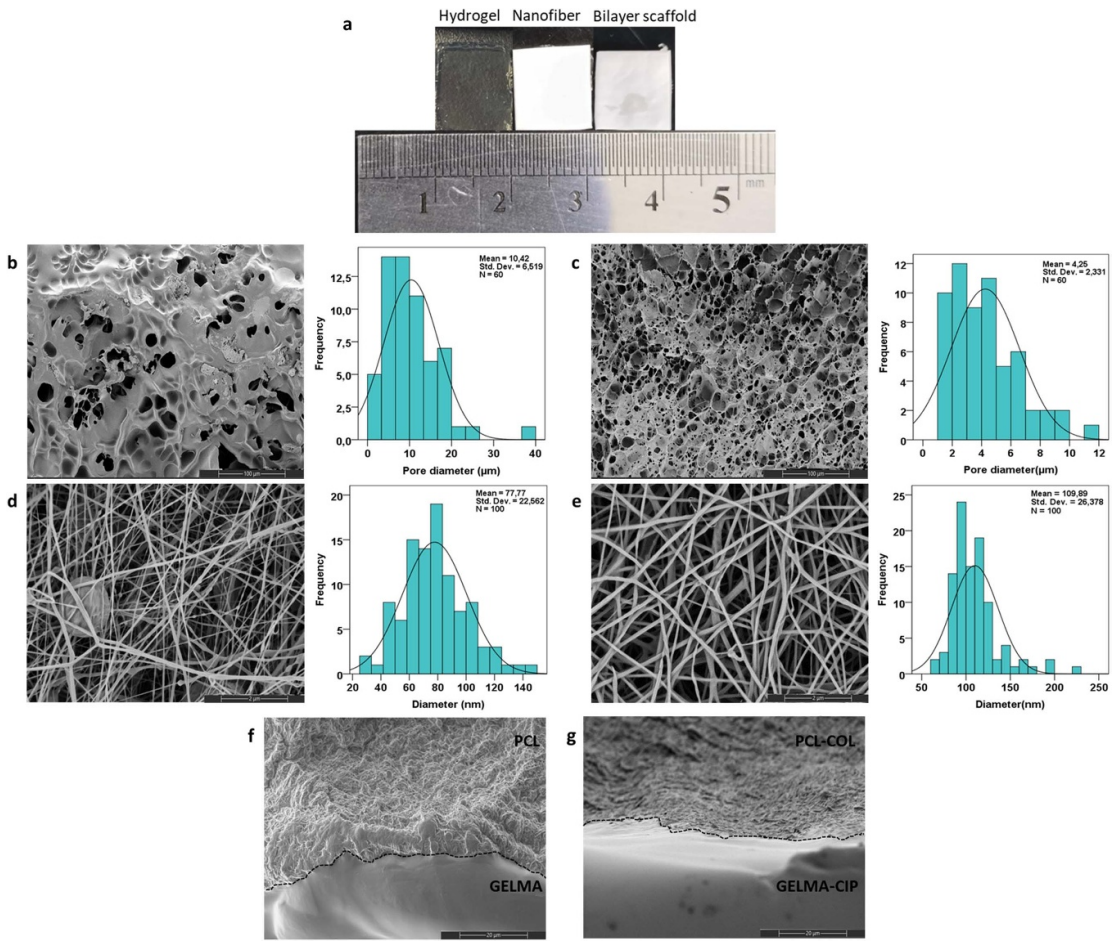

Figure 2. (a) The overall view of bilayer scaffolds composed of 3D-printed hydrogel and nanofiber patch SEM images of hydrogels, nanofibers and bilayer scaffolds: (b) GelMA hydrogel, (c) GelMA-CIP hydrogel, (d) PCL nanofibers, (e) PCL-COL nanofibers, (f) GelMA/PCL and (g) GelMA-CIP/PCL-COL.

use as drug delivery and tissue engineering scaffolds [36].

The surface morphology and the average fiber diameter of PCL and PCL-COL patches are demonstrated in figures 2(d) and (e). SEM images showed that PCL and PCL-COL fibers have a smooth surface and relatively uniform diameter with a bead-free structure. The average fiber diameters of PCL and PCL-COL electrospun nanofibers were measured as 77.77 ± 22.562 nm and 109.89 ± 26.378 nm, respectively. Increasing the polymer chain concentration in the PCL-COL solution caused the nanofiber diameter to increase. This result was also consistent with the literature [29, 37].

SEM images of the bilayer GelMA/PCL and GelMA-CIP/PCL-COL scaffolds are shown in figures 2(f) and (g). To show that both the hydrogel layer and the nanofiber layer were combined, the layers consisting of GelMA and GelMA-CIP hydrogels were not lyophilized. Based on the images, it was determined that the hydrogel layers and nanofiber layers successfully penetrated each other, as indicated by the border line. Because the hydrogel layer was wet and the nanofiber layer was thin, the two layers easily adhered to each other without any adhesive. This situation can be seen in the SEM images. It may be related to the rapid physical crosslinking of PCL and PCL-COL polymers with the free amine group present on the surface of GelMA and GelMA-CIP [3]. As shown in figures 2(f) and (g), the bilayer scaffold proposed in this study can be considered as a suitable candidate to mimic the extracellular structure.

3.2. Fourier transform infrared spectroscopy

Figure 3(a) presents the FTIR spectra of CIP, gelatin, GelMA, and GelMA-CIP hydrogels. In the CIP spectrum, a prominent peak was found between 3350 and 3300 cm^{-1}, characterizing the stretching vibration of O–H groups and intermolecular hydrogen bonding. Between 1000 and 1700 cm^{-1} the presence of a large number of double-bonded functional groups is detected. The peak between 1650 and 1600 cm^{-1} characterizes our antibiotic, which belongs to the quinolones. The peak between 1400 and 1350 cm^{-1} represents (C=O). It shows the bending vibration of the O–H group and proves the presence of the carboxylic

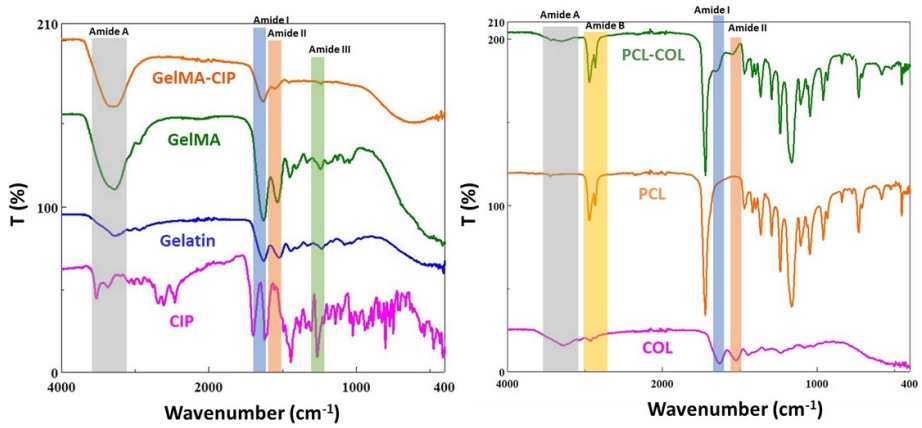

Figure 3. FTIR spectra showing the Amide A, Amide I, Amide II, and Amide III regions: (a) CIP, Gelatin, GelMA, and GelMA-CIP hydrogels, (b) COL, PCL, and PCL-COL nanofibers.

acid peak at 1250–1200 cm^{-1} [38]. In the GelMA spectrum, the peak at 3278 cm^{-1} is associated with the presence of peptide bonds O–H and N–H functional groups (Amide A) [39]. The absorption band at 1630 cm^{-1} is associated with the C=O stretching groups (Amide I) and the peak at 1535 cm^{-1} is associated with the N–H bending groups (Amide II). The amide II band in gelatin shifted to 1535 cm^{-1} in GelMA [40]. The absorption band at 1242 cm^{-1} is C–N stretching and N–H bending (Amide III). Due to the overlap of the characteristic bands of CIP and GelMA and the very small amount of drug in the GelMA-CIP hydrogel, we can say that slight shifts in the GelMA-CIP peaks compared to GelMA indicate the presence of CIP.

FTIR spectra of COL, PCL, and PCL-COL nanofibers are shown in figure 3(b). The spectrum of the COL showed a peak associated with N–H stretching at 3285 cm^{-1} (Amide A). Amide A band occurs due to O–H and N–H stretching. Amide B is associated with C–H stretching at 2927 cm^{-1} [41]. Amide I and II bands were detected at 1628 and 1524 cm^{-1}, respectively [42]. Amide I is formed due to C–H carbonyl stretching. Amide II is formed related to vibrations on the plane of the N–H bond and C–N stretching, and Amide III is due to C–N stretching and N–H deformation [43]. In the PCL spectrum, the 1722 cm^{-1} peak represents the stretching in the carbonyl group of the C=O ester. The peaks between 2943 cm^{-1} represent the strain in the structure of the C–H groups in the polymer [44]. Amide groups were observed in COL and PCL-COL nanofibers. Slight shifts were observed in the FTIR spectra of PCL-COL compared to the spectra of PCL. This can be explained by the low amount of COL in PCL.

3.3. Mechanical characterization of scaffolds

The mechanical properties of the nanofiber layer and the bilayer scaffold were evaluated by tensile experiments, while the mechanical performance of the hydrogel layer was characterized by the compression experiment [6]. Since the GelMA layer could not be placed between the jaws of the tester and tensile analysis could not be performed, compression analysis was performed. The mechanical properties of GelMA and GelMA-CIP depend on the combined effects of various factors such as degree of crosslinking, pore size and porosity [3]. The compressive strength of GelMA and GelMA-CIP hydrogels was calculated to be 24.46 $\pm$ 0.85 kPa and 13.61 $\pm$ 0.74 kPa, respectively (figures 4(a)–(c) and table 1). The decrease in mechanical properties and physiological stability of GelMA hydrogel after the addition of CIP may be due to gaps between polymer chains [45]. Thus, it can be concluded that the polymer cross-links of GelMA hydrogel are higher than those of GelMA-CIP, resulting in a mechanically stronger hydrogel. In addition, the increase in compressive strength of the hydrogel is an indication that it can withstand external pressure when implanted in the defect area [46]. Furthermore, this layer showed compressive strength values close to the soft tissues [47].

The tensile strength of PCL and PCL-COL hydrogels was calculated to be 0.88 $\pm$ 0.22 MPa and 3.32 $\pm$ 0.26 MPa, respectively (figures 4(d)–(f) and table 1). When COL was added to PCL nanofibers, the tensile strength of COL increased [48, 49]. The significant increase in tensile strength of the nanofibers by adding COL to PCL nanofibers can be interpreted as the ability of COL to absorb energy against the load due to its high degree of elongation [48]. It is also thought that this may be due to COL binding to PCL, which increases the fiber diameter. This is thought to contribute positively to the mechanical behavior. The tensile strength for cartilage tissue has been reported to be 1.1–2.5 MPa [50]. In addition, the tensile strength of various nerves has been reported to be in the range of 2–10 MPa [51].

The bilayer scaffold obtained by incorporating nanofibers into hydrogels also resulted in an increase

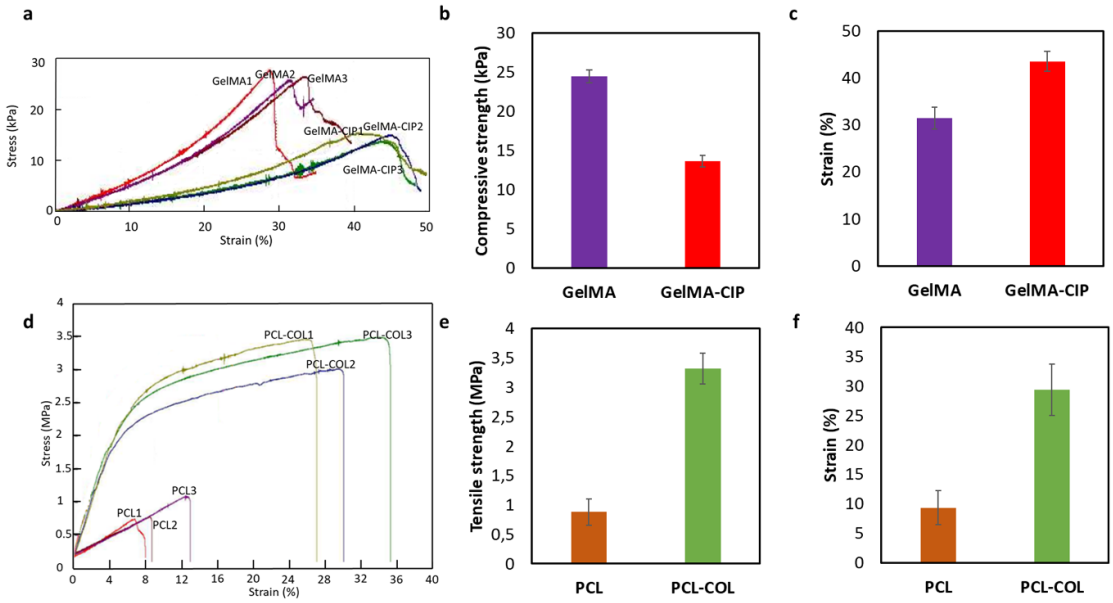

Figure 4. Compressive properties of GelMA and GelMA-CIP hydrogels: (a) for the compressive property, the stress-strain curve (b) compressive strength and (c) strain (%). Tensile properties of PCL and PCL-COL nanofibers: (d) for the tensile property, the stress-strain curve (e) tensile strength and (f) strain (%). Data are expressed as mean ± standard deviation (SD, $n = 3$).

Table 1. Mechanical test results of the scaffolds (Data are expressed as mean ± standard deviation (SD, $n = 3$)).

Scaffolds	Compressive strength (kPa)	Tensile strength (MPa)	Strain at break (%)
GelMA	24.46 ± 0.85	—	18.16 ± 3.47
GelMA-CIP	13.61 ± 0.74	—	13.50 ± 3.48
PCL	—	0.88 ± 0.22	9.32 ± 2.88
PCL-COL	—	3.32 ± 0.26	29.41 ± 4.39
GelMA/PCL	—	0.37 ± 0.13	27.72 ± 12.26
GelMA-CIP/PCL-COL	—	0.61 ± 0.27	37.90 ± 12.44

in the elongation at break, while the modulus of elasticity significantly decreased. This can be attributed to the 3D structure of the nanofibers in the bilayer scaffold [3]. It has been observed that the mechanical performance increases with the addition of nanofibers to the hydrogel groups. The mechanical strengths of GelMA/PCL and GelMA-CIP /PCL-COL are 0.37 ± 0.13 MPa and 0.61 ± 0.27 MPa, respectively. The high mechanical strength of the bilayer scaffold composed of GelMA-CIP/PCL-COL can be attributed to the highest mechanical properties of the PCL-COL nanofiber. It can be concluded that the nanofiber contributes to maintaining the mechanical integrity of the hydrogels [4]. The tensile strength for heart muscle and vessels is about 60–100 kPa and 300 kPa–3 MPa, respectively [52]. Given these values, it can be concluded that the mechanical properties of both the bilayer scaffold and its individual layers, as indicated by the results in table 1 and figure 5, fall within the tensile strength range of various tissues.

3.4. Swelling and degradation behavior of scaffolds

The swelling and degradation capacity are critical for the strength of the scaffolds and the release of the charge during the recovery period. To investigate swelling behavior, GelMA and GelMA-CIP hydrogels were incubated in PBS (pH 7.4) at 37 °C for 90 min to measure mass changes over time (figure 6(a)). It was observed that the swelling rate of the hydrogels increased significantly within the first 5 min. Swelling equilibrium was reached in 45 min for GelMA hydrogels and in 60 min for GelMA-CIP hydrogels. It was seen that the swelling rate of GelMA (∼341%) is lower than that of GelMA-CIP (∼413%). The greater number of cross-links in GelMA hydrogels provides less space for water to be retained during swelling, resulting in lower swelling rates. Similarly, the increase in the number of pores in the morphological structure of the GelMA-CIP hydrogel due to the increase in space between the polymer chains with the addition of CIP can be attributed to the fact that it forms fewer cross-links. Therefore, GelMA-CIP is likely to swell by absorbing more water [53, 54].

In order to accurately determine the period during which scaffolds degrade and trigger new tissue formation, degradation must be studied within a narrow range [48]. GelMA and GelMA-CIP hydrogels were incubated in PBS (pH 7.4) for 21 d at 37 °C and their degradation behavior was examined at certain time intervals (figure 6(b)). GelMA hydrogels

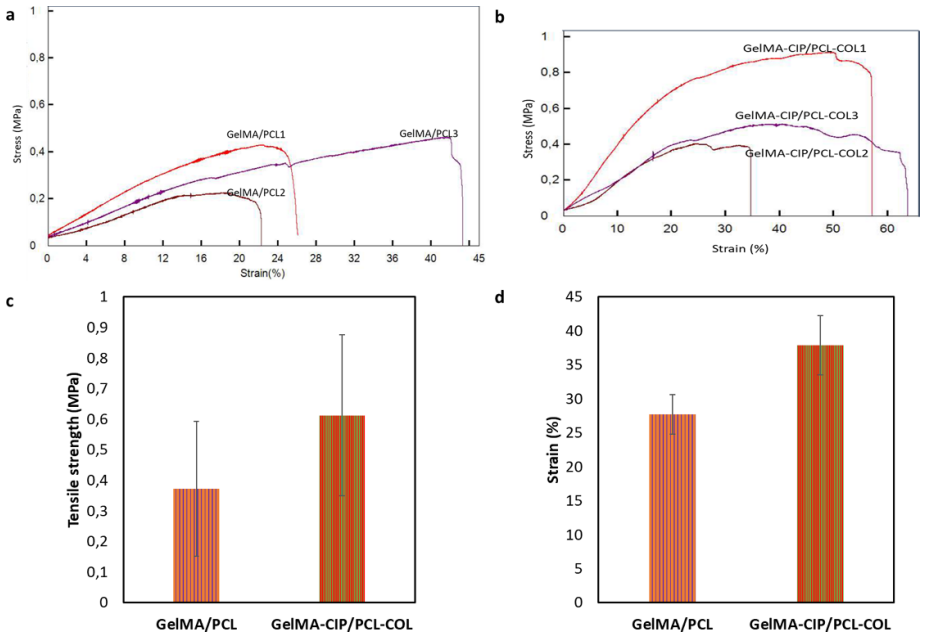

Figure 5. Tensile properties of bilayer scaffolds: (a) and (b) for the tensile property, the stress-strain curve (c) tensile strength and (d) strain (%). Data are expressed as mean ± standard deviation (SD, $n = 3$).

showed a ∼34% degradation rate at the end of 21 d, while GelMA-CIP hydrogels showed a ∼39% degradation rate. The degradation is likely to be consistent with the swelling results. In other words, GelMA hydrogels with more crosslinked areas are more resistant to degradation, while GelMA-CIP hydrogels with weaker polymeric crosslinks are more susceptible to degradation [54]. As a result, this can be attributed to the fact that the morphological, mechanical, and swelling properties of the hydrogels are consistent with each other.

The swelling abilities of PCL and PCL-COL nanofibers were studied by incubating them in PBS at 37 °C for 96 h, as presented in figure 6(c). PCL nanofibers reached swelling equilibrium at the 5th hour, while PCL-COL nanofibers reached equilibrium at the 1st hour. At the end of the 96th hour, the swelling rate of PCL-COL nanofibers was ∼136%, while the swelling rate of PCL fibers was ∼110%. As a result, it was observed that the swelling ratio of PCL-COL fibers increased compared to PCL fibers. This was interpreted as an increase in hydrophilicity [25] with the addition of COL to the hydrophobic PCL and, consequently, an increase in swelling rate.

PCL nanofibers were found to be more stable than PCL/COL nanofibers when incubated in a PBS solution at 37 °C for 21 d. At the end of the 21st day, PCL/COL showed a degradation of ∼23%, while PCL showed a degradation of ∼6% (figure 6(d)). With the addition of COL to PCL nanofibers, swelling and degradation rates increased [29]. Because PCL is crystalline and COL is an amorphous polymer, the amorphous region decomposes faster than the crystalline region during hydrolytic degradation [48].

Swelling equilibrium was reached in 60 min for GelMA/PCL bilayer scaffold and in 90 min for the GelMA-CIP/PCL-COL bilayer scaffold (figure 6(e)). It was found that the swelling rate of GelMA/PCL (∼411%) is higher than that of GelMA-CIP/PCL-COL (∼340%). The presence of more physical bonds in GelMA-CIP/PCL-COL compared to GelMA/PCL is likely due to the COL content in its structure, which may have influenced the swelling properties of the bilayer scaffolds. When the mechanical properties and swelling behavior of the bilayer scaffolds were evaluated together, they were found to be compatible.

3.5. *In vitro* drug release study

In vitro drug release studies were performed to investigate the release behavior of CIP from GelMA-CIP hydrogels. To mimic the physiological conditions of living organisms, the test was performed in PBS (pH 7.4, 37 °C) for 48 h. UV absorbance at 278 nm was used to detect the released CIP. UV spectra obtained with the concentration range of CIP from 0.2 to 1 μg ml^{-1} were plotted, and a linear standard calibration curve was constructed from the CIP absorbance values ($R^2 = 0.9975$) (figures 7(a) and (b)). GelMA-CIP hydrogels showed a 70% burst release of CIP from the hydrogels within the first 1 h of incubation, as shown in figure 7(c). At the end of 48 h, 100% release of the drug was achieved. There may be multiple reasons for the rapid release of drugs from hydrogels. The increased number of pores on the surface of GelMA-CIP can be attributed to accelerated drug release. There is a direct relationship between swelling behavior and drug release. This may also partially cause the burst release. Another reason may be

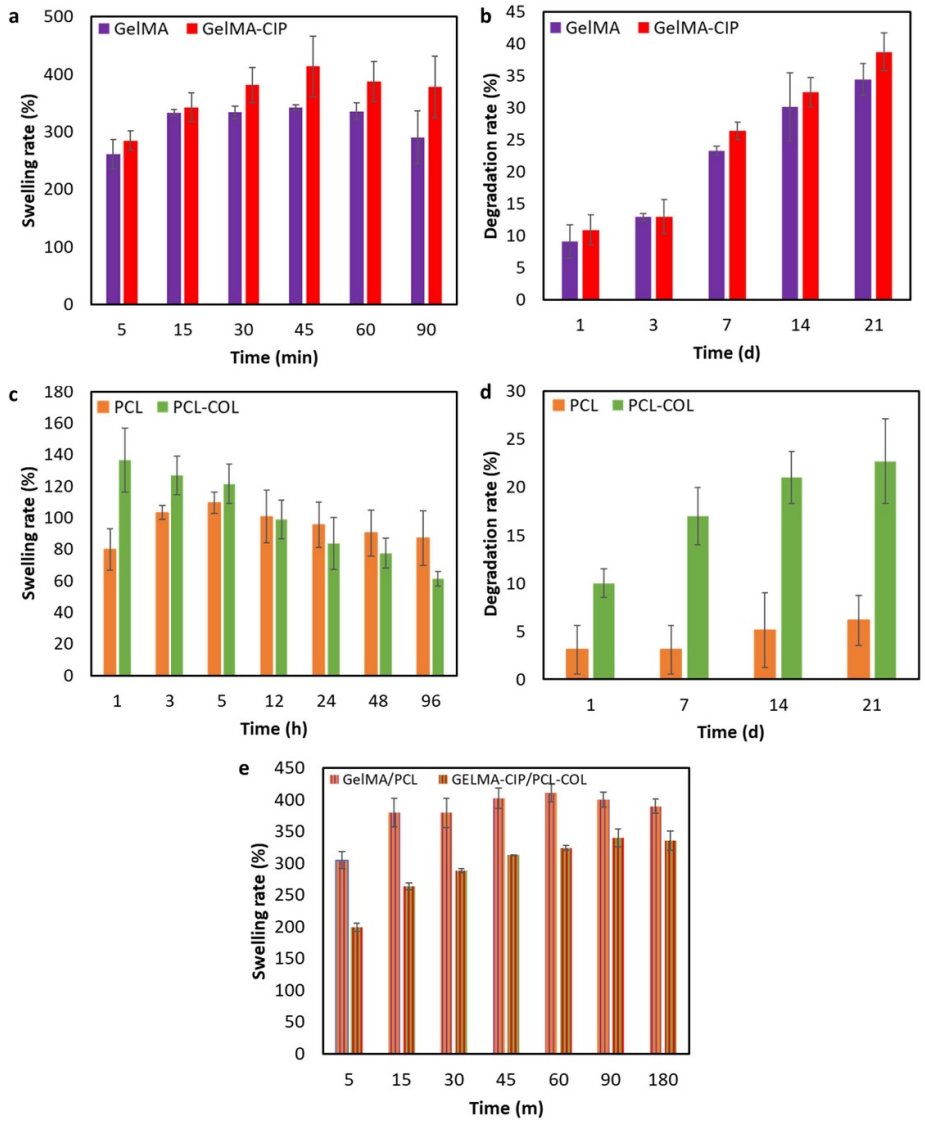

Figure 6. (a) Swelling and (b) degradation behavior of GelMA and GelMA-CIP hydrogels. (c) Swelling and (d) degradation behavior of PCL and PCL-COL nanofibers. (e) Swelling behavior of Bilayer scaffolds. Data are expressed as mean ± standard deviation (SD, $n = 3$).

the use of too few antibiotics. In fact, Vigata *et al* showed that drug release time can be directly proportional to the amount of drug [55]. In order to increase the drug release time, the loading of the drug into the hydrogel can be varied. For example, Khalil *et al* [45] developed micelles containing CIP and released 80% of the drug in 12 h. Ribeiro *et al* [56] incorporated nanofibers prepared with CIP and β-cyclodextrin complex into GelMA hydrogels by cryocutting method and observed significantly higher drug release at the end of the first day than the groups without the complex.

3.6. *In vitro* antibacterial activity

Antimicrobial analysis was performed on the GelMA-CIP layer of the bilayer scaffold. GelMA and GelMA-CIP hydrogels (containing 30, 100, 250, and 500 µl antibiotic solution) were monitored for the number of zones created compared to the positive control. According to the antibacterial results, the zone of inhibition around GelMA-CIP (500 µl) showed activity against all bacteria. GelMA containing 30, 100, 250 µl of CIP and empty GelMA did not show antibacterial activity against *S. aureus* and *P. aeruginosa* bacteria (figure 8). The inhibition zone diameters determined from GelMA and GelMA-CIP hydrogels are detailed in table 2.

3.7. *In vitro* cell viability

Cell viability was measured by MTT analysis in both the bilayer scaffold and the scaffold-forming groups. The cytocompatibility was evaluated in hydrogels, nanofibers, and bilayer scaffolds incubated with cells for 1, 3, and 7 d, as shown in figure 9. The results were compared with the negative control. All groups showed an average cell viability of over 70%, which was accepted as the biomaterial being non-cytotoxic according to ISO 10993-5. The higher cell viability

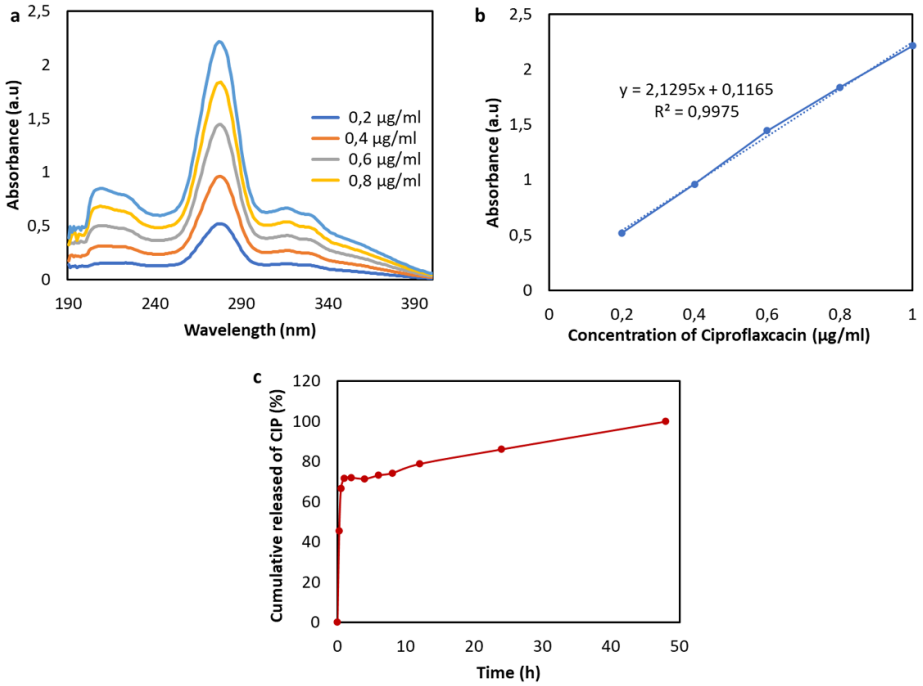

Figure 7. *In vitro* drug release profile of GelMA-CIP hydrogels: (a) Absorption spectra of CIP at different concentrations, (b) the calibration curve of CIP, (c) CIP release behavior from GelMA-CIP hydrogels.

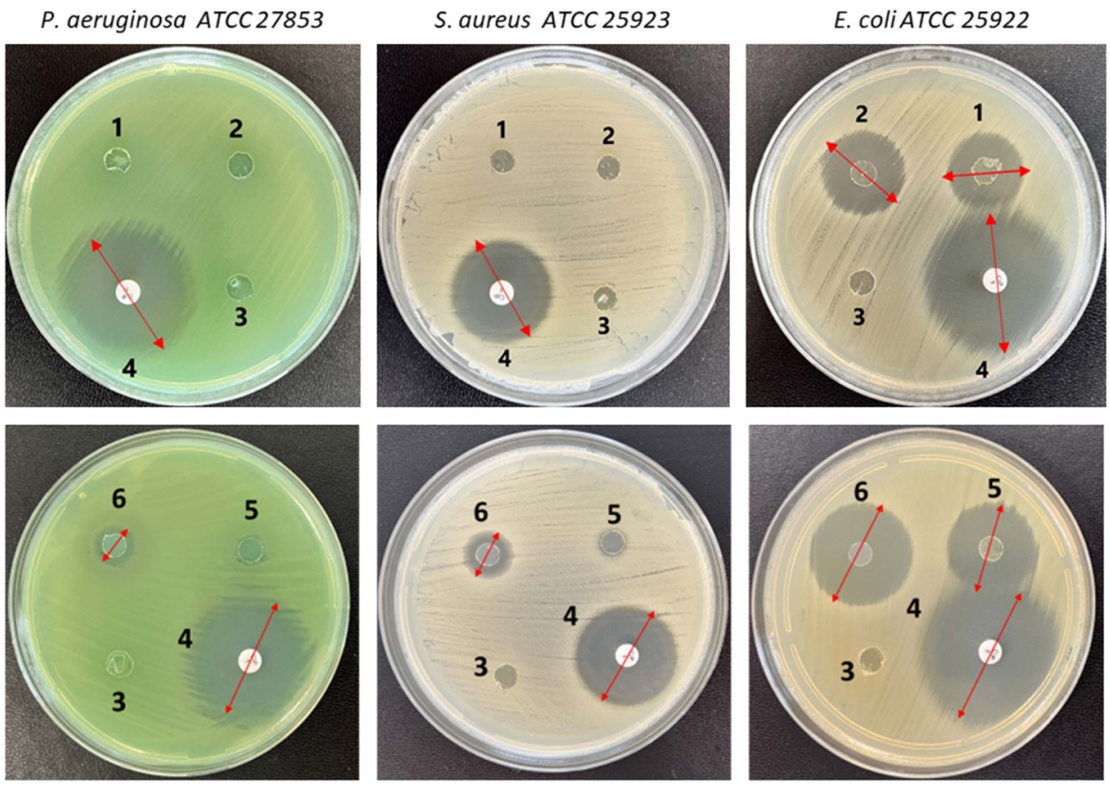

Figure 8. Antibacterial of GelMA and GelMA-CIP (30, 100, 250, and 500 µl) against *S. aureus, P. aeruginosa,* and *E. coli.*

of GelMA-CIP (94%) compared to GelMA (78%) hydrogel at the end of day 7 can be attributed to the higher number of pores on the surface of GelMA-CIP hydrogel. Because more porous hydrogels or hydrogels with larger pore sizes can accelerate cell growth, migration, and proliferation [53]. PCL-COL nanofiber showed 106% cell viability at the end of day 7, while GelMA-CIP/PCL-COL showed 102% cell viability. It was observed that the COL-contained groups (PCL-COL and GelMA-CIP/PCL-COL) showed a

Table 2. Inhibition zone diameters (mm) of GelMA and GelMA-CIP (30, 100, 250, and 500 µl) against *S. aureus, P. aeruginosa*, and *E. coli*.

	1 (30 µl CIP)	2 (100 µl CIP)	3 (GelMA)	4 (CIP disk) (5 µg)	5 (250 µl CIP)	6 (500 µl CIP)
P. aeruginosa 27 853	—	—	—	35	—	12
S. aureus 25 923	—	—	—	27	—	13
E. coli 25 922	—	20	23	—	25	28

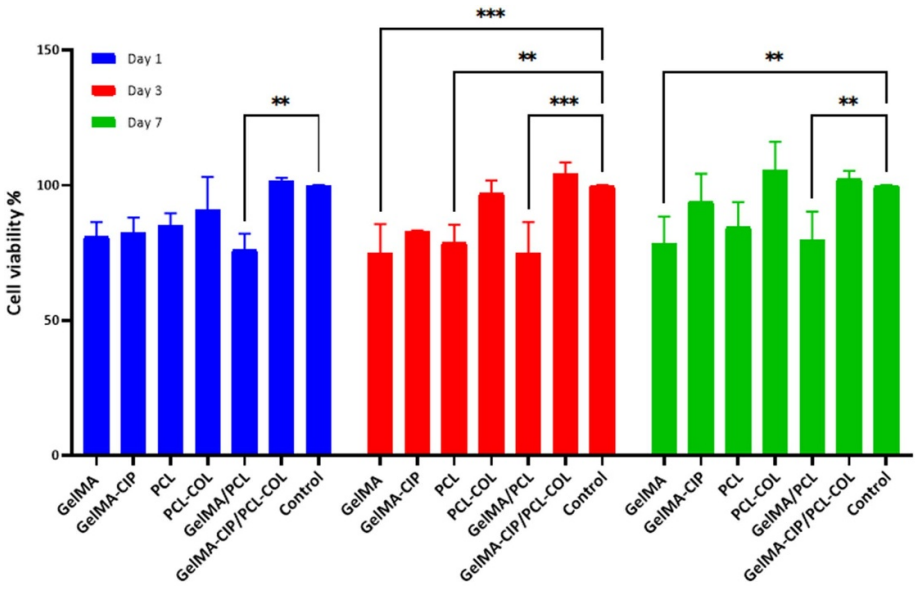

Figure 9. Cell viability results of 1-day, 3-day, and 7-day treated hydrogels, nanofibers and bilayer scaffolds.

proliferative effect on cell viability compared to other groups that do not contain COL, confirming the effect of biomaterials developed with COL on cell viability [57, 58]. In addition, it can be interpreted that cell adhesion and proliferation are faster due to the synergistic effect between the PCL carboxyl group and the COL amino group [48]. Both the physiological similarity of the nanofibers to native ECM and the presence of COL contributed in part to the positive interaction between cells and nanofiber scaffolds. Thus, the positive effect of COL-developed biomaterials on cell viability was confirmed [57, 58]. All results were evaluated by a two-way analysis of variance (ANOVA) using Dunnett's multiple comparison test. No statistical significance was found in the COL groups compared to the control, but $^{**}p < 0.01$ and $^{***}p < 0.001$ were found to be significant in the GelMA/PCL groups compared to the control on all days. Data are expressed as mean ± SD for all groups and are statistically significant compared to controls. Statistical analysis was performed using GrapPhad Prism 9 software.

4. Conclusions

To summarize the study, the fabrication of the hydrogel/electrospun nanofiber bilayer scaffold, which we predicted would be used in many tissue engineering applications, was successfully confirmed by chemical and morphological analysis. Although the addition of CIP altered some physical and mechanical properties of GelMA-CIP hydrogels, the hydrogel was shown to have pore diameter, compressive strength (24.46 ± 0.85 kPa), antimicrobial properties, and cytocompatibility (>70%) suitable for biomedical application. Similarly, the PCL-COL nanofiber was shown to have adequate tensile strength (3.32 ± 0.26 MPa) and cytocompatibility (∼106%). A new scaffold with synergistic effects was designed with the GelMA-CIP/PCL-COL bilayer scaffold, where the cytocompatibility (∼102%).

A new scaffold with synergistic effects with appropriate tensile strength (0.61 ± 0.27 MPa), swelling (∼340%), and cytocompatibility (∼102%) was designed with the GelMA-CIP/PCL-COL bilayer scaffold.

Thus, the limits of the application of hydrogels and electrospun material composites alone in the tissue engineering field have been tried to be overcome. Bilayer scaffolds obtained from electrospun nanofibers prepared by combining 3D-printed GelMA hydrogels will give a dynamic direction to the treatment methods of tissue parts with very complex structures in the future.

Data availability statement

All data that support the findings of this study are included within the article (and any supplementary files).

Acknowledgments

This study was supported by Yıldız Technical University under BAP program with ADEP Project. The Project Number is TSA-2022-5244. Hilal YILMAZ has been supported by both the Higher Education Council (YÖK) 'Biomedical Technology and Equipment (Design-Manufacturing and Supply)', the YÖK 100/2000 Doctoral Program, and the Turkish Scientific and Technical Research Council (TUBITAK) BIDEP 2211-A 2020/2. We would also like to thank Rabia Betul Sulutas and Yagmur Kazancioglu for their assistance.

ORCID iDs

Hilal Yilmaz https://orcid.org/0000-0003-3326-4873
Cem Bulent Ustundag https://orcid.org/0000-0002-4439-0878

References

[1] Ng W L, Goh M H, Yeong W Y and Naing M W 2018 Applying macromolecular crowding to 3D bioprinting: fabrication of 3D hierarchical porous collagen-based hydrogel constructs *Biomater. Sci.* **6** 562–74
[2] Rose J C and De Laporte L 2018 Hierarchical design of tissue regenerative constructs *Adv. Healthcare Mater.* **7** 1701067
[3] Hajiabbas M, Alemzadeh I and Vossoughi M 2020 A porous hydrogel-electrospun composite scaffold made of oxidized alginate/gelatin/silk fibroin for tissue engineering application *Carbohydrate Polym.* **245** 116465
[4] Zhang M *et al* 2023 Electrospun nanofiber/hydrogel composite materials and their tissue engineering applications *J. Mater. Sci. Technol.* **162** 157–78
[5] Xu T, Binder K W, Albanna M Z, Dice D, Zhao W, Yoo J J and Atala A 2012 Hybrid printing of mechanically and biologically improved constructs for cartilage tissue engineering applications *Biofabrication* **5** 015001
[6] Miguel S P, Cabral C S D, Moreira A F and Correia I J 2019 Production and characterization of a novel asymmetric 3D printed construct aimed for skin tissue regeneration . *Colloids Surf.* B **181** 994–1003
[7] Ng W L, Lee J M, Zhou M, Chen Y-W, Lee K-X A, Yeong W Y and Shen Y-F 2020 Vat polymerization-based bioprinting—process, materials, applications and regulatory challenges *Biofabrication* **12** 022001
[8] Kidalov S, Voznyakovskii A, Vozniakovskii A, Titova S and Auchynnikau Y 2023 The effect of few-layer graphene on the complex of hardness, strength, and thermo physical properties of polymer composite materials produced by digital light processing (DLP) 3D printing *Materials* **16** 1157
[9] Zhu W, Ma X, Gou M, Mei D, Zhang K and Chen S 2016 3D printing of functional biomaterials for tissue engineering *Curr. Opin. Biotechnol.* **40** 103–12
[10] Zhou F *et al* 2020 Rapid printing of bio-inspired 3D tissue constructs for skin regeneration *Biomaterials* **258** 120287
[11] Thrasher C J, Schwartz J J and Boydston A J 2017 Modular elastomer photoresins for digital light processing additive manufacturing *ACS Appl. Mater. Interfaces* **9** 39708–16
[12] Ye W *et al* 2020 3D printing of gelatin methacrylate-based nerve guidance conduits with multiple channels *Mater. Des.* **192** 108757
[13] Kumar H, Sakthivel K, Mohamed M G A, Boras E, Shin S R and Kim K 2021 Designing gelatin methacryloyl (GelMA)-based bioinks for visible light stereolithographic 3D biofabrication *Macromol. Biosci.* **21** 2000317
[14] Dong Y, Zhang M, Han D, Deng Z, Cao X, Tian J and Ye Q 2022 A high-performance GelMA–GelMA homogeneous double-network hydrogel assisted by 3D printing *J. Mater. Chem.* B **10** 3906–15
[15] Song P *et al* 2022 DLP fabricating of precision GelMA/HAp porous composite scaffold for bone tissue engineering application *Composites* B **244** 110163
[16] Gao J, Wang H, Li M, Liu Z, Cheng J, Liu X, Liu J, Wang X and Zhang L 2023 DLP-printed GelMA-PMAA scaffold for bone regeneration through endochondral ossification *Int. J. Bioprint.* **9** 754
[17] Qian Y *et al* 2023 DLP printed hDPSC-loaded GelMA microsphere regenerates dental pulp and repairs spinal cord *Biomaterials* **299** 122137
[18] Shen J, Song W, Liu J, Peng X, Tan Z, Xu Y, Liu S and Ren L 2024 3D bioprinting by reinforced bioink based on photocurable interpenetrating networks for cartilage tissue engineering *Int. J. Biol. Macromol.* **254** 127671
[19] Joshi A, Kaur T, Joshi A, Gugulothu S B, Choudhury S and Singh N 2022 Light-mediated 3D printing of micro-pyramid-decorated tailorable wound dressings with endogenous growth factor sequestration for improved wound healing *ACS Appl. Mater. Interfaces* **15** 327–37
[20] Sharma G K and James N R 2022 Electrospinning: the technique and applications *Recent Developments in Nanofibers Research* (Intechopen)
[21] Dippold D, Cai A, Hardt M, Boccaccini A R, Horch R, Beier J P and Schubert D W 2017 Novel approach towards aligned PCL-Collagen nanofibrous constructs from a benign solvent system *Mater. Sci. Eng.* C **72** 278–83
[22] Gautam S, Purohit S D, Singh H, Dinda A K, Potdar P D, Sharma C, Chou C-F and Mishra N C 2023 Surface modification of PCL-gelatin-chitosan electrospun scaffold by nano-hydroxyapatite for bone tissue engineering *Mater. Today Commun.* **34** 105237
[23] Kim H *et al* 2021 Improved chondrogenic performance with protective tracheal design of Chitosan membrane surrounding 3D-printed trachea *Sci. Rep.* **11** 1–8
[24] Lashkari M *et al* 2023 Cell-based wound dressing: bilayered PCL/gelatin nanofibers-alginate/collagen hydrogel scaffold loaded with mesenchymal stem cells *Int. J. Biol. Macromol.* **239** 124099
[25] She Y, Fan Z, Wang L, Li Y, Sun W, Tang H, Zhang L, Wu L, Zheng H and Chen C 2021 3D printed biomimetic PCL scaffold as framework interspersed with collagen for long segment tracheal replacement *Front. Cell Dev. Biol.* **9** 629796
[26] Ding H, Cheng Y, Niu X and Hu Y 2020 Application of electrospun nanofibers in bone, cartilage and osteochondral tissue engineering *J. Biomater. Sci.* **32** 536–61
[27] Doodmani S M, Bagheri A, Natouri O, Nobakht A and Saghebasl S 2024 Electrospinning-netting of spider-inspired polycaprolactone/collagen nanofiber-nets incorporated with Propolis extract for enhanced wound healing applications *Int. J. Biol. Macromol.* **267** 131452
[28] Lu X, Zou H, Liao X, Xiong Y, Hu X, Cao J, Pan J, Li C and Zheng Y 2022 Construction of PCL-collagen@ PCL@ PCL-gelatin three-layer small diameter artificial vascular grafts by electrospinning *Biomed. Mater.* **18** 015008
[29] Huo P, Han X, Zhang W, Zhang J, Kumar P and Liu B 2021 Electrospun nanofibers of polycaprolactone/collagen as a sustained-release drug delivery system for artemisinin *Pharmaceutics* **13** 1228
[30] Sharma P C, Jain A, Jain S, Pahwa R and Yar M S 2010 Ciprofloxacin: review on developments in synthetic, analytical, and medicinal aspects *J. Enzyme Inhib. Med. Chem.* **25** 577–89

[31] Campoli-Richards D M, Monk J P, Price A, Benfield P, Todd P A and Ward A 1988 Ciprofloxacin: a review of its antibacterial activity, pharmacokinetic properties and therapeutic use *Drugs* **35** 373–447
[32] Seidi A, Ramalingam M, Elloumi-Hannachi I, Ostrovidov S and Khademhosseini A 2011 Gradient biomaterials for soft-to-hard interface tissue engineering *Acta Biomater.* **7** 1441–51
[33] Baykara D, Bedir T, Ilhan E, Mutlu M E, Gunduz O, Narayan R and Ustundag C B 2023 Fabrication and optimization of 3D printed gelatin methacryloyl microneedle arrays based on vat photopolymerization *Front. Bioeng. Biotechnol.* **11** 1157541
[34] Tang L *et al* 2023 GelMA hydrogel loaded with extracellular vesicles derived from umbilical cord mesenchymal stem cells for promoting cutaneous diabetic wound healing *ACS Omega* **8** 10030–9
[35] Bakravi A, Ahamadian Y, Hashemi H and Namazi H 2018 Synthesis of gelatin-based biodegradable hydrogel nanocomposite and their application as drug delivery agent *Adv. Polym. Technol.* **37** 2625–35
[36] Thang N H, Chien T B and Cuong D X 2023 Polymer-based hydrogels applied in drug delivery: an overview *Gels* **9** 523
[37] Kanani A G and Bahrami S H 2011 Effect of changing solvents on poly (ε-caprolactone) nanofibrous webs morphology *J. Nanomater.* **2011** 1–10
[38] Khan M Z H, Aziz M A, Hasan M R and Al-Mamun M R 2016 The role of drug as corrosion inhibitor for mild steel surface characterization by SEM, AFM, and FTIR *Anti-Corros. Methods Mater.* **63** 308–15
[39] Erkus H, Bedir T, Kaya E, Tinaz G B, Gunduz O, Chifiriuc M-C and Ustundag C B 2023 Innovative transdermal drug delivery system based on amoxicillin-loaded gelatin methacryloyl microneedles obtained by 3D printing *Materialia* **27** 101700
[40] Jamshidifar E, Esfandyari-Manesh M, Motasadizadeh H, Naderizadeh S, Yourdkhani A, Samadi N and Dinarvand R 2022 Improvement of *in vitro* osteogenesis and anti-infection properties by GelMA scaffold containing levofloxacin nanoparticles and strontium microspheres for osteomyelitis *J. Mater. Sci.* **57** 13603–19
[41] Ghosal K, Thomas S, Kalarikkal N and Gnanamani A 2014 Collagen coated electrospun polycaprolactone (PCL) with titanium dioxide (TiO_2) from an environmentally benign solvent: preliminary physico-chemical studies for skin substitute *J. Polym. Res.* **21** 1–5
[42] Riaz T, Zeeshan R, Zarif F, Ilyas K, Muhammad N, Safi S Z, Rahim A, Rizvi S A A and Rehman I U 2018 FTIR analysis of natural and synthetic collagen *Appl. Spectrosc. Rev.* **53** 703–46
[43] Júnior Z S S, Botta S B, Ana P A, França C M, Fernandes K P S, Mesquita-Ferrari R A, Deana A and Bussadori S K 2015 Effect of papain-based gel on type I collagen-spectroscopy applied for microstructural analysis *Sci. Rep.* **5** 11448
[44] Öztel O N, Yılmaz H, Isoglu I A and Allahverdıyev A 2023 Investigation of the interaction of adipose-derived mesenchymal stem cells with ε-polycaprolactone and egg white scaffolds *Gazi Univ. J. Sci.* **36** 1434–47
[45] Khalil I A, Saleh B, Ibrahim D M, Jumelle C, Yung A, Dana R and Annabi N 2020 Ciprofloxacin-loaded bioadhesive hydrogels for ocular applications *Biomater. Sci.* **8** 5196–209
[46] Choi J-B, Kim Y-K, Byeon S-M, Park J-E, Bae T-S, Jang Y-S and Lee M-H 2021 Fabrication and characterization of biodegradable gelatin methacrylate/biphasic calcium phosphate composite hydrogel for bone tissue engineering *Nanomaterials* **11** 617
[47] Singh G and Chanda A 2021 Mechanical properties of whole-body soft human tissues: a review *Biomed. Mater.* **16** 062004
[48] Zhang Q, Lv S, Lu J, Jiang S and Lin L 2015 Characterization of polycaprolactone/collagen fibrous scaffolds by electrospinning and their bioactivity *Int. J. Biol. Macromol.* **76** 94–101
[49] Hackett J M, Dang T, Tsai E and Cao X 2010 Electrospun biocomposite polycaprolactone/collagen tubes as scaffolds for neural stem cell differentiation *Materials* **3** 3714–28
[50] Vahedi P, Jarolmasjed S, Shafaei H, Roshangar L, Soleimani Rad J and Ahmadian E 2019 In vivo articular cartilage regeneration through infrapatellar adipose tissue derived stem cell in nanofiber polycaprolactone scaffold *Tissue Cell* **57** 49–56
[51] Zarei M, Samimi A, Khorram M, Abdi M M and Golestaneh S I 2021 Fabrication and characterization of conductive polypyrrole/chitosan/collagen electrospun nanofiber scaffold for tissue engineering application *Int. J. Biol. Macromol.* **168** 175–86
[52] Lv S, Dudek D M, Cao Y, Balamurali M M, Gosline J and Li H 2010 Designed biomaterials to mimic the mechanical properties of muscles *Nature* **465** 69–73
[53] Suvarnapathaki S, Nguyen M A, Wu X, Nukavarapu S P and Camci-Unal G 2019 Synthesis and characterization of photocrosslinkable hydrogels from bovine skin gelatin *RSC Adv.* **9** 13016–25
[54] Ren P, Wei D, Liang M, Xu L, Zhang T and Zhang Q 2022 Alginate/gelatin-based hybrid hydrogels with function of injecting and encapsulating cells in situ *Int. J. Biol. Macromol.* **212** 67–84
[55] Vigata M, O'Connell C D, Cometta S, Hutmacher D W, Meinert C and Bock N 2021 Gelatin methacryloyl hydrogels for the localized delivery of cefazolin *Polymers* **13** 3960
[56] Ribeiro J S, Daghrery A, Dubey N, Li C, Mei L, Fenno J C, Schwendeman A, Aytac Z and Bottino M C 2020 Hybrid antimicrobial hydrogel as injectable therapeutics for oral infection ablation *Biomacromolecules* **21** 3945–56
[57] Zhang Y, Venugopal J, Huang Z-M, Lim C T and Ramakrishna S 2005 Characterization of the surface biocompatibility of the electrospun PCL-collagen nanofibers using fibroblasts *Biomacromolecules* **6** 2583–9
[58] Fu W, Liu Z, Feng B, Hu R, He X, Wang H, Yin M, Huang H, Zhang H and Wang W 2014 Electrospun gelatin/PCL and collagen/PLCL scaffolds for vascular tissue engineering *Int. J. Nanomed.* **9** 2335–44